

# Using H II region spectra to probe the ionizing radiation from massive stars

S. Simón-Díaz<sup>1,3</sup>, J. García-Rojas<sup>2</sup>, G. Stasińska<sup>3</sup> and C. Esteban<sup>4</sup>

<sup>1</sup>Observatoire de Genève, <sup>2</sup>Universidad Nacional Autónoma de México

<sup>3</sup>LUTH, Observatoire de Paris, Site de Meudon, <sup>4</sup>Instituto de Astrofísica de Canarias

**Abstract.** We present some results of an on-going project aimed at studying a sample of Galactic H II regions ionized by a single massive star to test the predictions of modern generation stellar atmosphere codes in the H Lyman continuum. The observations collected for this study comprise the optical spectra of the corresponding ionizing stars, along with imaging and long-slit spatially resolved nebular observations. The analysis of the stellar spectra allows to obtain the stellar parameters of the ionizing star, while the nebular observations provide constraints on the nebular abundances and gas distribution. All this information is then used to construct tailored photoionization models of the H II regions. The reliability of the stellar ionizing fluxes is hence tested by comparing the photoionization model results with the observations in terms of the spatial variation across the nebula of an appropriate set of nebular line ratios.

**Keywords.** stars: atmospheres, stars: early-type, stars: individual (HD 37061, BD +45 3216), HII regions, ISM: individual (M 43, Sh 2-112)

---

## 1. Motivation

In the last decades, a great effort has been devoted to the development of stellar atmosphere codes for massive stars. The advent of the new generation of NLTE, line blanketed model atmosphere codes, either plane-parallel (TLUSTY, Hubeny & Lanz, 1995), or spherically expanded (FASTWIND, Puls et al. 2005; CoSTAR, Schaerer & de Koter 1997; CMFGEN, Hillier & Miller 1998; WM-*basic*, Pauldrach et al. 2001) is already a fact. Each of them uses specific approximations in the calculation of the stellar atmosphere structure and spectral energy distribution (SED).

This new generation of stellar atmosphere models produce quite different ionizing SEDs from the ones produced by the previous plane-parallel, hydrostatic models (either LTE by Kurucz 1991, or NLTE by e.g. Mihalas & Auer 1970). Some notes on this, and on the consequences on the ionization structure of H II regions, can be found in Gabler et al. (1989), Najarro et al. (1996), Sellmaier et al. (1996), Rubin et al. (1995), and Stasińska & Schaerer (1997). Although the new predictions seem to go in the right direction (viz. Giveon et al. 2002, Morisset et al. 2004) non-negligible differences can still be found between the various stellar codes (see e.g. Mokiem et al. 2004, Martins et al. 2005, Puls et al. 2005).

Since the FUV range of the stellar flux cannot be observed directly, it is crucial to find indirect tests to constrain it. Ionized nebulae have many times been claimed as potential tools to check the validity of the emergent SED predicted by the stellar atmosphere models. Here we consider the possibility of using tailored models of simple, spatially resolved Galactic H II regions ionized by single massive stars to this aim. In this work we present preliminary results for two apparently spherical Galactic H II regions (M 43 and Sh 2-112) to illustrate the capabilities of the methodology we have developed.

## 2. Nebular candidates: the Galactic HII regions M 43 and Sh2-112

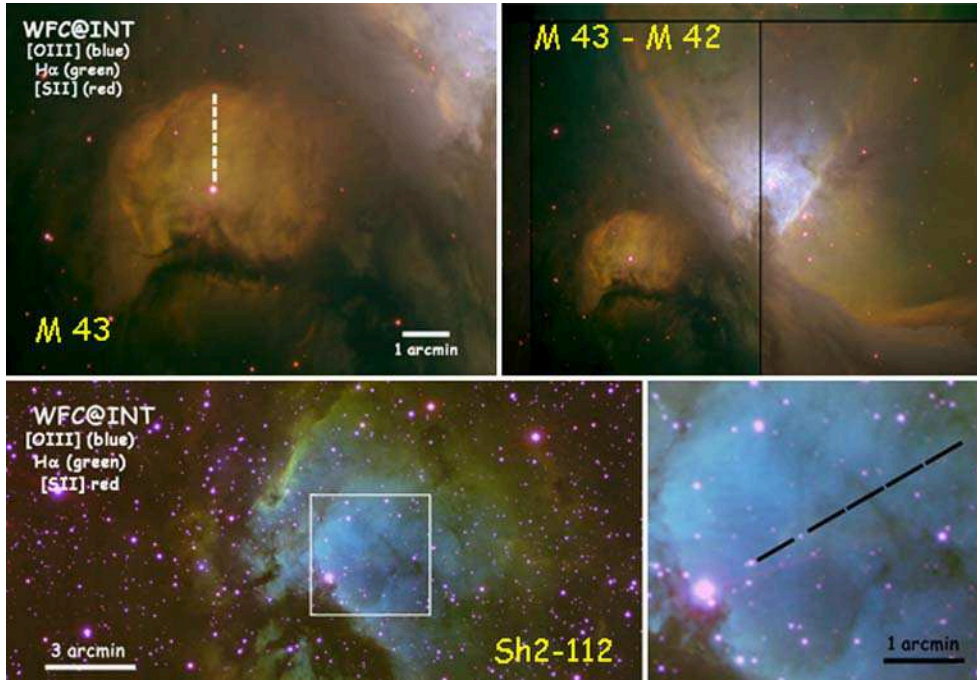


**Figure 1.** WFC images of the Galactic HII regions M 43 (up) and Sh 2-112 (down), showing the location of the small apertures obtained from the long-slit used for the nebular spectroscopy. The ionizing stars of these nebulae are HD 37061 (B0.5 V) and BD +35 4216 (O8 V), respectively. Note the proximity of M 43 to the Orion Nebula (M 42) in the upper right image.

## 3. The observational dataset

STELLAR SPECTROSCOPY	NEBULAR IMAGING	LONG-SLIT NEBULAR SPECTROSCOPY
<u>IDS@INT2.5</u>	<u>WFC@INT2.5m</u>	<u>ISIS@WHT4.2m</u>
<u>H2400B (R=7500)</u>	Narrow band filters:	<u>R600B (<math>\delta\lambda = 2.25 \text{ \AA}</math>)</u>
$\lambda_{\text{range}}: [4000 - 4550] \text{ \AA}$	H $\alpha$ , H $\beta$ , [SII], [OIII]	$\lambda_{\text{range}}: [3880 - 5146] \text{ \AA}$
$\lambda_{\text{range}}: [4500 - 5050] \text{ \AA}$	Spatial resolution:	<u>R316R (<math>\delta\lambda = 4.65 \text{ \AA}</math>)</u>
<u>H1800V (R=8500)</u>	0.33 arcsec/pix	$\lambda_{\text{range}}: [5100 - 7520] \text{ \AA}$
$\lambda_{\text{range}}: [6350 - 6750] \text{ \AA}$	FOV: 33 x 33 arcmin	$\lambda_{\text{range}}: [7300 - 9720] \text{ \AA}$
SNR = 200 - 300		Slit length*: 3.5 arcmin
* Nebular spectroscopy is obtained extracting small size apertures from the long-slit		Slit width: 1.5 arcsec

**Table 1:** Summary of the observational dataset characteristics

## 4. Detailed spectroscopic analysis of the ionizing stars: HD 37061 and BD+45 3216

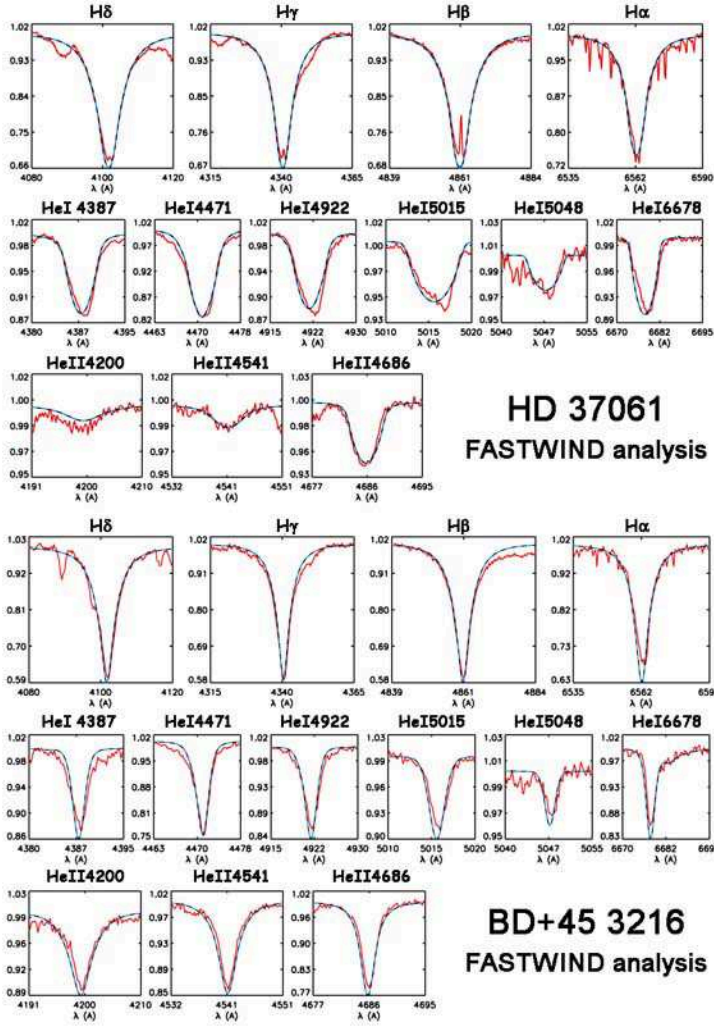


**Figure 2.** The stellar parameters of the ionizing stars were determined by means of the fit of the H, He I-II observed profiles with FASTWIND synthetic profiles convolved with the instrumental and rotational profiles (see Tables 1, 2a-b). In the case of BD +35 4216 an extra-broadening (i.e. macroturbulence) was needed to properly fit the observed lines.

**HD 37061 (B0.5 V)**

$m_v = 6.84 \pm 0.01$	$v \sin i = 200 \pm 20 \text{ km/s}$	
$A_v = 2.09 \pm 0.03$	$T_{\text{eff}} = 31 \pm 1 \text{ kK}$	$R/R_{\odot} = 5.7 \pm 0.9$
$d = 400 \pm 50 \text{ pc}$	$\log g = 4.1 \pm 0.1$	$\log(L/L_{\odot}) = 4.43 \pm 0.13$
$\Rightarrow M_v = -3.3 \pm 0.3$	$\xi_{\text{rot}} = 5 \text{ km/s}$	$M/M_{\odot} = 14 \pm 6$
	$\log Q = -13.5$	$\log Q(H^{\beta}) = 47.1$

**BD +45 3216 (O8 V)**

$m_v = 9.07 \pm 0.01$	$(v \sin i, \Theta_{\tau}) = (50, 90) \text{ km/s}$	
$A_v = 1.99 \pm 0.29$	$T_{\text{eff}} = 37.5 \pm 1.0 \text{ kK}$	$R/R_{\odot} = 7.2 \pm 1.7$
$d = 1.74 \pm 0.17 \text{ Kpc}$	$\log g = 4.1 \pm 0.1$	$\log(L/L_{\odot}) = 4.95 \pm 0.21$
$\Rightarrow M_v = -4.1 \pm 0.5$	$\xi_{\text{rot}} = 5 \text{ km/s}$	$M/M_{\odot} = 24 \pm 12$
	$\log Q = -13.5$	$\log Q(H^{\beta}) = 48.4$

**Tables 2a-b:** Results from the spectroscopic analysis of the stars. Photometric data and distances to the stars, used to estimate their stellar radii, luminosities and masses, are also indicated.

## 5. Comparing the ionizing SEDs predicted by the various stellar atmosphere codes

As a first step, we compared the predictions — in terms of the shape of the ionizing SEDs — of the four modern stellar atmosphere codes CMFGEN, WM-*basic*, FASTWIND, and TLUSTY. To this aim we specifically calculated models with the various stellar codes, using the same stellar parameters (those indicated in Tables 2a-b), and the solar set of abundances from Grevesse & Sauval (1998).

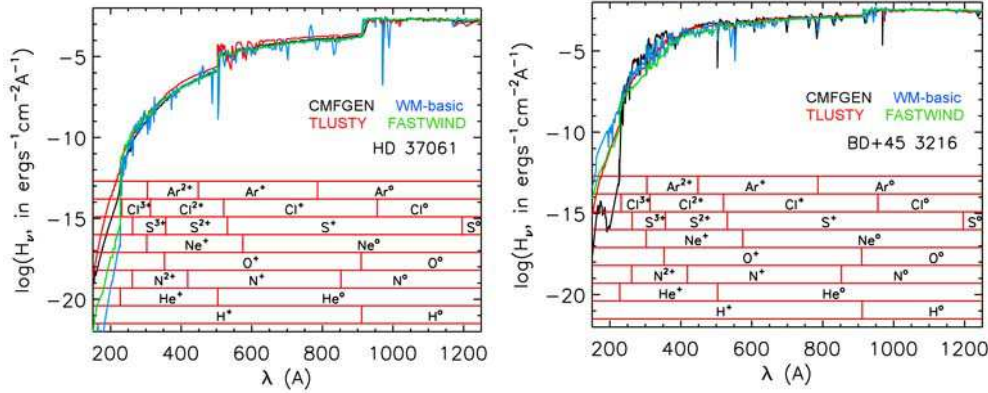


**Figure 3.** Comparison of ionizing SEDs from CMFGEN, WM-*basic*, FASTWIND, and TLUSTY models with the stellar parameters indicated in Tables 2a-b. All SEDs have been re-mapped to the same  $\lambda$ -grid for a better comparison.

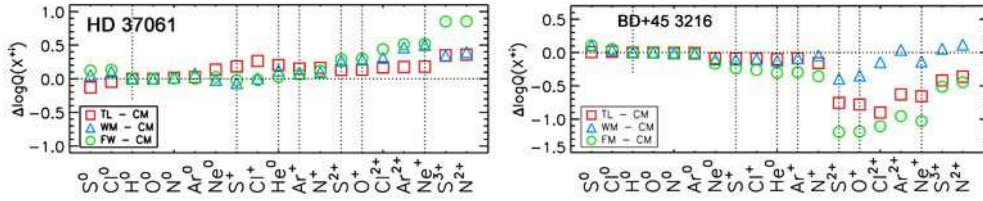


**Figure 4.** To quantify the differences showed by Figs. 3, we plot the quantity  $\Delta \log Q(X^{+i})$  for the ions indicated in those figures, using a scale in which  $\Delta \log Q(H^0)=0$ . This type of diagram gives us an idea of how the shape of the SEDs compares in the H Lyman continuum. Alternatively, the number of ionizing photons for the various ionic species relative to the total number of  $H^0$  ionizing photons can be compared (see its utility in Sect. 6).

There are several ingredients which can affect the ionizing SED predictions:

- (a) The ionization structure of the stellar atmosphere
- (b) The blocking of emergent flux by the large amount of weak metal lines present in this spectral region (line blocking) and its effect over the ionization structure of the stellar atmosphere (line blanketing)
- (c) The presence of strong resonant lines (either in absorption or emission)
- (d) The presence of a velocity field in the stellar atmosphere

All these effects must be taken into account when comparing the ionizing SED. Depending of the spectral region, the importance of each one of them can be more or less important.

## 6. The stellar - nebular connexion

The state of ionization of a nebula depends, in first approximation, on the ionization parameter ( $U$ ), and the hardness of the ionizing radiation. Following Vilchez & Pagel (1988):

$$\frac{n(X^{i+1})}{n(X^i)} \propto U \frac{\int_{\nu(X^i)}^{\infty} \frac{H_\nu}{h\nu} d\nu}{\int_{13.6\text{eV}}^{\infty} \frac{H_\nu}{h\nu} d\nu} \propto U \frac{Q(X^i)}{Q(H^0)}, \quad (6.1)$$

where  $n(X^{i+1})$  is the number density of the  $i$ -times ionized atom of element  $X$ , and  $H_\nu$  is the stellar Eddington flux. Therefore, a ratio  $n(X^{i+1})/n(X^i)$  is, to a first approach and for a given  $U$ , proportional to the number of photons able to ionize  $X^i$  relative to that of the Lyman continuum photons.

Therefore, we can use nebular line ratios involving lines from to successive ions of the same element (i.e. giving the ionization degree of the nebula) as constraints of the ionizing stellar SEDs at various wavelengths. These are indicated in Table 3.

## 7. Some useful nebular line ratios

N <sub>e</sub> diagnostic		T <sub>e</sub> diagnostic	
[S II] 6731	6716	[N II] 5755	6584
Ionization degree			
[S III] 9069	HeI 6678	[O III] 5007	Optical
[S II] 6731	Hβ	[O II] 3727+	IR
[Ar III] 9.0	[N III] 57.2	[S IV] 10.5	[Ne III] 15.5
[Ar II] 7.0	[N II] 121.7	[S III] 18.7	[Ne II] 12.8
Nebular abundances			
[Ne III] 3869	[S III] 9069	[O III] 5007	[Ar III] 7135
Hβ	Hβ	Hβ	Hβ
HeI 6678	[S II] 6731	[O II] 3727+	[N II] 6584
Hβ	Hβ	Hβ	Hβ

**Table 3:** List of some useful nebular line ratios indicating the nebular physical properties ( $T_e$ ,  $N_e$ , and ionization degree) and abundances. The color code is the same as the one used in Figs 5 and 6.

## 8. Tailored photoionization models: probing the ionizing SED predictions

We then constructed photoionization models for the nebulae, using the ionizing SEDs commented in Sec. 5. We used CLOUDY (v02.07.01, Ferland et al. 1998). Tables 4a-b summarize the characteristics of the CLOUDY models. The nebular abundances were initially derived by means of the usual nebular techniques (i.e. direct method), and then fine-tuned to fit the observational constraints.

Figs. 5 and 6 compare the photoionization model results (as a function of the projected distance to the central star) with the nebular observational data obtained from the various apertures.

M43 (CLOUDY models)		Sh2-112 (CLOUDY models)	
Stellar SEDs from CMFGEN, TLUSTY, WM-basic and FASTWIND models with $T_{\text{eff}}=31$ Kk $\log g=4.1$ $\log Q(\text{H}^0) = 47.1$		Stellar SEDs from CMFGEN, TLUSTY, WM-basic and FASTWIND models with $T_{\text{eff}}=37.5$ Kk $\log g=4.0$ $\log Q(\text{H}^0) = 48.4$	
Spherical constant density models	Nebular abundances ( $\log X/\text{H}$ )	Spherical constant density models	Nebular abundances ( $\log X/\text{H}$ )
$N_{\text{H}} = 600 \text{ cm}^{-3} (= N_{\text{H}}[\text{SII}])$ $R_{\text{int}} = 10^{16} \text{ cm}$ Dust free	He = -1.01, N = -4.32, O = -3.70, Ne = -4.30, S = -5.10, Ar = -6.00	$N_{\text{H}} = 20 \text{ cm}^{-3} (= N_{\text{H}}[\text{SII}])$ $R_{\text{int}} = 10^{16} \text{ cm}$ Dust free	He = -0.95, N = -4.50, O = -3.56, Ne = -4.22, S = -5.16, Ar = -5.90

Tables 4a-b: Input parameters used for the CLOUDY photoionization models.

**M43:** The output from photoionization models using SEDs from the various stellar codes are very similar, except for the  $[\text{S III}]/[\text{S II}]$  line ratio (as expected from the comparison of the quantity  $Q(\text{S}^+)/Q(\text{H}^0)$  in Fig. 4). The observational constraints point towards predictions from the spherical models; unfortunately, the nebular spectrum of M43 is contaminated by an external nebular emission (as can be noticed from the behavior of the  $[\text{O III}]/\text{H}\alpha$ ,  $[\text{Ne III}]/\text{H}\alpha$ , and  $[\text{O III}]/[\text{O II}]$  line ratios in the outer part of the nebula), not allowing to achieve a firm conclusion. The behavior of these line ratios may be explained by assuming that the nearby O7 V star  $\theta^1$  Ori C (the ionizing source of M 42; see Fig. 1) is ionizing the nebular material in front of M43. This contamination is clearly noticed when considering lines from  $\text{O}^{2+}$  and  $\text{Ne}^{2+}$ , since these lines are expected to be emitted by M43 itself only in a small region close to the ionizing star (due to the low temperature of HD 37061), but other lines may also be affected.

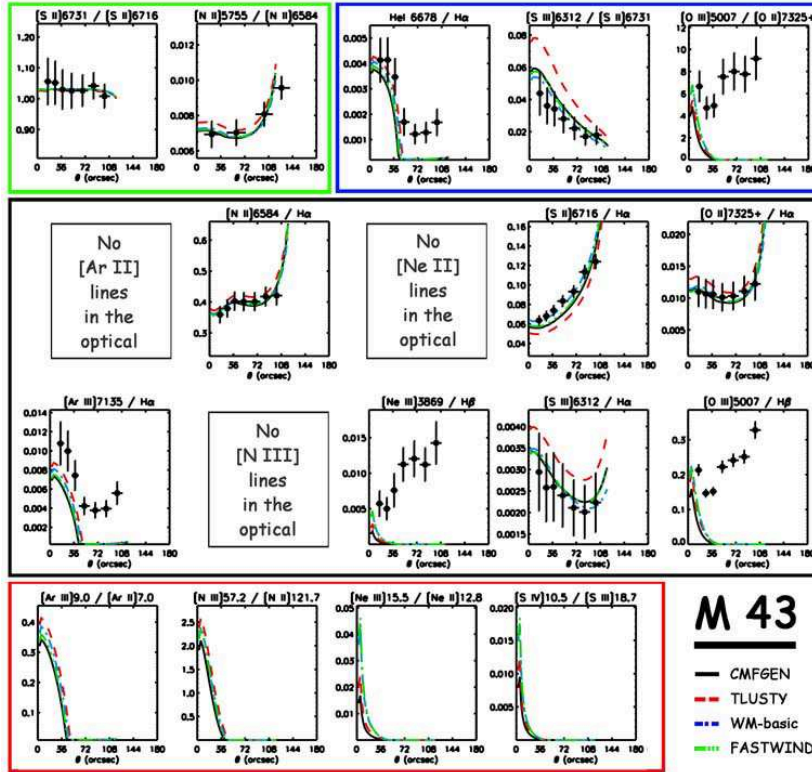


Figure 5. Comparison of the output from the photoionization models with the nebular spectroscopic observations for the case of M43.

**Sh2-112:** In this case, photoionization models show that nebular results are very different depending on the considered SED. It is interesting to see how results presented in Fig. 6 (concerning the nebular ionization degree constraints) and Fig. 4 are related. Note the importance of the IR line ratios in this case (except for the optical [O III] / [O II] line ratio, it is the only way to test the stellar SEDs for  $\lambda \leq 430 \text{ \AA}$ ).

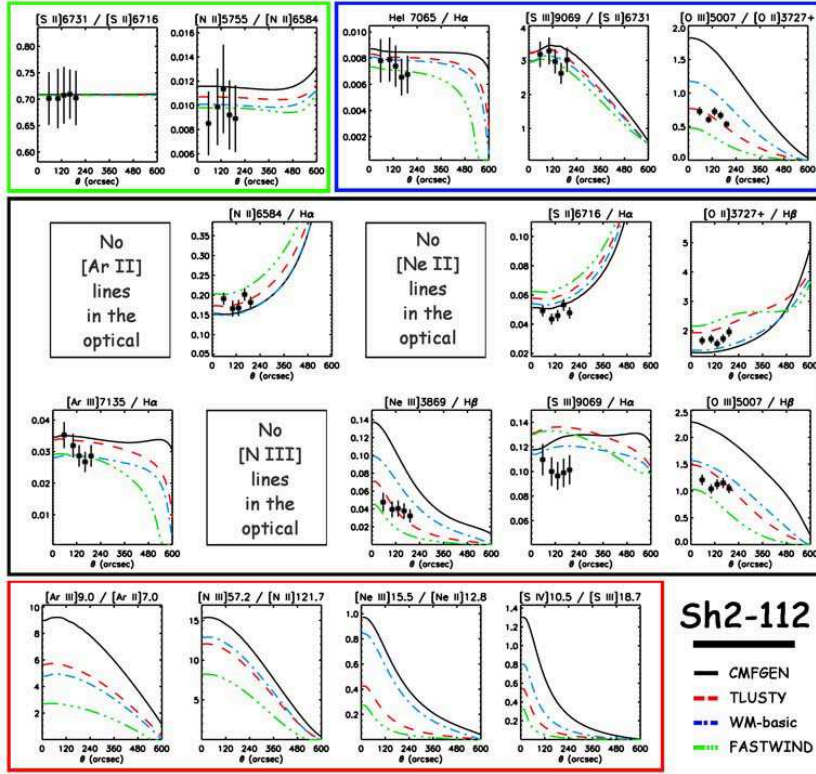


Figure 6. As Fig. but for the case of Sh2-112.

## 9. A final note

- We have shown that the methodology presented here (based on a combined stellar-nebular study of spatially resolved HII regions ionized by a single massive star) is very promising regarding the study of the reliability of the ionizing SEDs predicted by stellar atmosphere codes.
- We have presented here results using simple dust free constant density spherical models representing the nebular gas, but we are also exploring the effect of considering dust, more complicated nebular gas distributions, and the possible escape of ionizing photons in the models. It is important to test the effect of these ingredients before proposing conclusions about the ionizing SED predictions.

## References

- Ferland, G. J., Korista, K. T., Verner, D. A., Ferguson, J. W., Kingdon, J. B., & Verner, E. M. 1998, *PASP*, 110, 761
- Gabler, R., Gabler, A., Kudritzki, R. P., Puls, J., & Pauldrach, A. 1989, *A&A*, 226, 162
- Giveon, U., Sternberg, A., Lutz, D., Feuchtgruber, H., & Pauldrach, A. W. A. 2002, *ApJ*, 566, 880
- Grevesse, N., & Sauval, A. J. 1998, *Space Science Reviews*, 85, 161
- Hillier, D. J., & Miller, D. L. 1998, *ApJ*, 496, 407
- Hubeny, I., & Lanz, T. 1995, *ApJ*, 439, 875
- Kurucz, R. L. 1991, *BAAS*, 23, 1047
- Martins, F., Schaerer, D., & Hillier, D. J. 2005, *A&A*, 436, 1049
- Mihalas, D., & Auer, L. H. 1970, *ApJ*, 160, 1161
- Mokiem, M. R., Martín-Hernández, N. L., Lenorzer, A., de Koter, A., & Tielens, A. G. G. M. 2004, *A&A*, 419, 319
- Morisset, C., Schaerer, D., Bouret, J.-C., & Martins, F. 2004, *A&A*, 415, 577
- Najarro, F., Kudritzki, R. P., Cassinelli, J. P., Stahl, O., & Hillier, D. J. 1996, *A&A*, 306, 892
- Pauldrach, A. W. A., Hoffmann, T. L., & Lennon, M. 2001, *A&A*, 375, 161
- Puls J., Urbaneja M., A., Venero R., et al. 2005, *A&A*, 435, 669
- Rubin, R. H., Kunze, D., & Yamamoto, T. 1995, *Astrophysical Applications of Powerful New Databases*, 78, 479
- Schaerer, D., & de Koter, A. 1997, *A&A*, 322, 598
- Sellmaier, F. H., Yamamoto, T., Pauldrach, A. W. A., & Rubin, R. H. 1996, *A&A*, 305, L37
- Stasińska, G., & Schaerer, D. 1997, *A&A*, 322, 615
- Vilchez, J. M., & Pagel, B. E. J. 1988, *MNRAS*, 231, 257

This figure "M43-3-photomodel.jpg" is available in "jpg" format from:

<http://arxiv.org/ps/0802.0016v1>

This figure "S112-3-photomodel.jpg" is available in "jpg" format from:

<http://arxiv.org/ps/0802.0016v1>

This figure "Dat\_M43.jpg" is available in "jpg" format from:

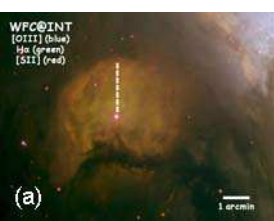
<http://arxiv.org/ps/0802.0016v1>

This figure "M43\_photons.jpg" is available in "jpg" format from:

<http://arxiv.org/ps/0802.0016v1>

This figure "M43\_rendijas.jpg" is available in "jpg" format from:

<http://arxiv.org/ps/0802.0016v1>



This figure "Dat\_S112.jpg" is available in "jpg" format from:

<http://arxiv.org/ps/0802.0016v1>

This figure "S112\_photons.jpg" is available in "jpg" format from:

<http://arxiv.org/ps/0802.0016v1>

This figure "Dat\_HD37061.jpg" is available in "jpg" format from:

<http://arxiv.org/ps/0802.0016v1>

This figure "HD37061\_fit.jpg" is available in "jpg" format from:

<http://arxiv.org/ps/0802.0016v1>

This figure "HD37061\_fluxes.jpg" is available in "jpg" format from:

<http://arxiv.org/ps/0802.0016v1>

This figure "BD453216\_fit.jpg" is available in "jpg" format from:

<http://arxiv.org/ps/0802.0016v1>

This figure "BD453216\_fluxes.jpg" is available in "jpg" format from:

<http://arxiv.org/ps/0802.0016v1>

This figure "Dat\_BD453216.jpg" is available in "jpg" format from:

<http://arxiv.org/ps/0802.0016v1>

This figure "WFC\_images\_rendijas.jpg" is available in "jpg" format from:

<http://arxiv.org/ps/0802.0016v1>

This figure "diagn.jpg" is available in "jpg" format from:

<http://arxiv.org/ps/0802.0016v1>

This figure "observa.jpg" is available in "jpg" format from:

<http://arxiv.org/ps/0802.0016v1>